

Incoherent Measurement of Sub-10 kHz Optical Linewidths

Félix Montjovet-Basset,¹ Jayash Panigrahi,¹ Diana Serrano,¹ Alban Ferrier,^{1,2}
Emmanuel Flurin,³ Patrice Bertet,³ Alexey Tiranov,¹ and Philippe Goldner^{1,*}

¹*Chimie ParisTech, PSL University, CNRS, Institut de Recherche de Chimie Paris, 75005 Paris, France*

²*Faculté des Sciences et Ingénierie, Sorbonne Université, UFR 933, 75005 Paris, France*

³*Quantronics group, Université Paris-Saclay, CEA, CNRS, SPEC, Gif-sur-Yvette Cedex, France*

(Dated: November 12, 2024)

Quantum state lifetimes T_2 , or equivalently homogeneous linewidths $\Gamma_h = 1/\pi T_2$, are a key parameter for understanding decoherence processes in quantum systems and assessing their potential for applications in quantum technologies. The most common tool for measuring narrow optical homogeneous linewidths, i.e. long T_2 , is the measurement of coherent photon echo emissions, which however gives very weak signal when the number of emitters is small. This strongly hampers the development of nano-materials, such as those based on rare earth ions, for quantum communication and processing. In this work we propose, and demonstrate in an erbium doped crystal, a measurement of photon echoes based on incoherent fluorescence detection and its variance analysis. It gives access to T_2 through a much larger signal than direct photon echo detection, and, importantly, without the need for a highly coherent laser. Our results thus open the way to efficiently assess the properties of a broad range of emitters and materials for applications in quantum nano-photonics.

Measuring quantum state lifetimes T_2 , or equivalently homogeneous linewidths $\Gamma_h = 1/\pi T_2$, is a fundamental tool for understanding decoherence processes in quantum systems. Of great interest for fundamental studies, it also provides the time during which quantum states can be used and is thus a crucial parameter for applications to quantum technologies.

In materials such as rare earth (RE) doped crystals at low temperatures, optical T_2 can be very long, corresponding to extremely narrow homogeneous linewidths from a few kHz down to 75 Hz [1]. Combined with long spin coherence times [2–5], this makes them promising systems for quantum memories [6–8], micro-wave to optical transduction [9], or single photon sources for quantum nodes [10–13]. Measuring such narrow homogeneous linewidths is however challenging since they are masked by the transitions' inhomogeneous broadening, i.e. the distribution of their frequencies due to varying micro-strain across the crystal structure [14].

In this case, the preferred technique for evaluating Γ_h is the photon echo (PE), an experiment directly derived from the ubiquitous spin or Hahn echo [15]. It enables monitoring the free evolution of the relative phases between the emitters' superposition states as a function of time. This evolution is directly related to T_2 and thus Γ_h and numerous studies have shown the efficiency of this technique for measuring Γ_h on a broad range of time scales and deciphering complex dynamics in RE doped crystals [14, 16, 17].

PE is a spontaneous collective coherent emission occurring after two laser pulses. Its intensity is independent of the coherence lifetime of the laser driving the emitters $T_{2,laser}$ as long as $T_{2,laser} > \tau_{laser}$ where τ_{laser} is the longest pulse length, typically on the order of a μ s [16]. This is a key advantage as $T_{2,laser}$ is often orders of magnitude shorter than the emitters' T_2 . In

stark contrast, techniques like spectral hole burning or saturation spectroscopy operate in the opposite domain, i.e. $T_{2,laser} \gg T_2$, and are thus much more demanding and in addition prone to experimental biases such as power broadening [14, 17, 18]. The energy released in the coherent PE emission is however only a small fraction of the total energy stored after excitation [19]. This is not a problem for bulk materials where the collective enhancement, proportional to the square of the number of emitters N , is large. It makes however direct measurements of PE emission very difficult when N becomes small. This is the case for nanostructured materials, like nanoparticles, thin films, and milled or implanted bulk crystals, which nevertheless offer unique possibilities for greatly enhanced light-matter coupling and integration into photonic circuits [5, 10–13, 20, 21]. To be able to measure PE in such systems, one has to apply an additional laser pulse at the PE emission time in order to convert the emitter's superposition states into excited or ground state populations, detect their fluorescence and in this way retrieve a large fraction of the stored energy [22]. However, the intensity of the incoherent fluorescence signal depends on the relative phase between the laser pulse and the PE, which suggests that a highly coherent laser has to be used.

In this work, we show that in fact homogeneous optical linewidths can be measured using detection of an incoherent signal as well as incoherent excitation. Using an Er^{3+} doped Y_2SiO_5 single crystal, a material actively investigated for quantum memories and single photon sources [3, 22, 23], we recorded a photon echo decay monitoring fluorescence which gives $T_2 = 37 \pm 2 \mu\text{s}$ or $\Gamma_h = 8.6 \pm 0.4 \text{ kHz}$. As $T_{2,laser} = 15 \pm 1 \mu\text{s}$, the laser used was indeed mostly incoherent on the time scale of PE decay. This was achieved by measuring the fluorescence intensity variance instead of mean value [24] of only ≈ 2500

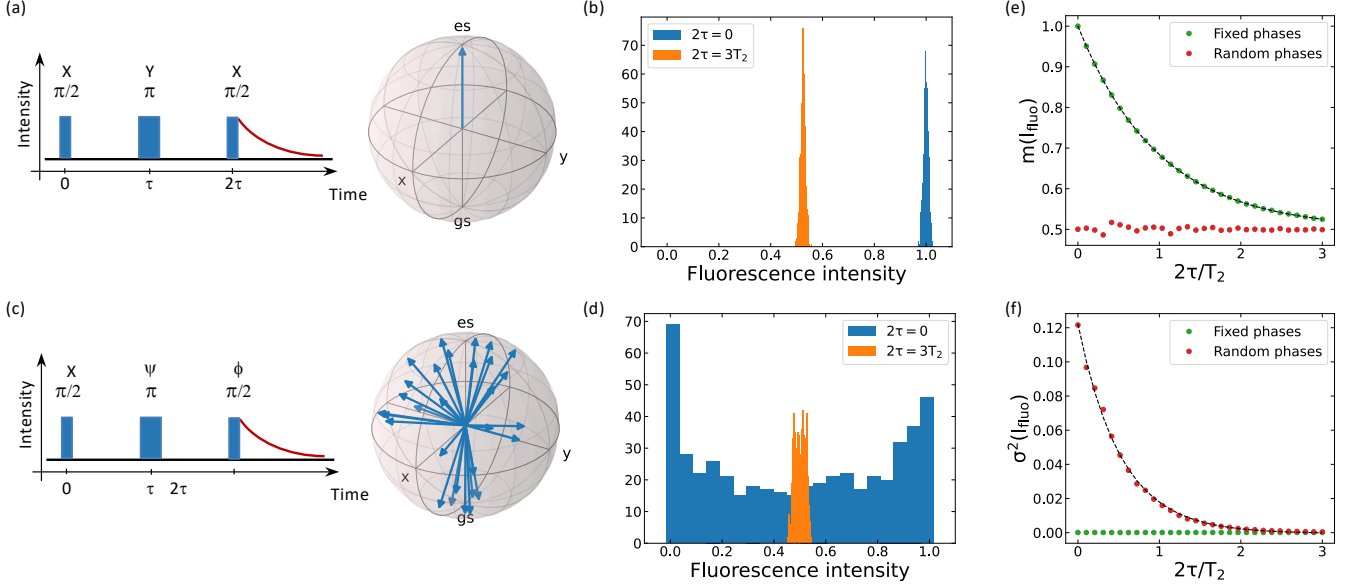


FIG. 1. Principle of fluorescence-detected photon echoes (PE). (a) PE sequence with fixed $X - Y - X$ phases for the three laser pulses. Fluorescence (red line) is integrated after the last $\pi/2$ pulse which converts coherences into populations. For evolution times $2\tau \ll T_2$, the final state after the last $\pi/2$ pulse is the excited state (es), as shown in the Bloch sphere. (b) Histogram of the integrated fluorescence intensity (I_{fluor}) for sequence (a) and different evolution times. A gaussian noise ($\sigma = 0.01$) has been added to I_{fluor} and $T_2 \ll T_1$ is assumed. (c) Same sequence as in (a) but with randomly varying phases ψ and ϕ . The final state on the Bloch sphere is a random vector. (d) Histogram of I_{fluor} for sequence (c). (e,f) Mean (m) and variance (σ^2) of I_{fluor} , normalized to N and N^2 (see text), for sequences (a), fixed phases, and (b), random phases. Exponential fits of σ^2 and m for (a) and (c) respectively (black lines) result in the same value of T_2 (see text).

ions. Our results demonstrate a new tool to probe narrow optical homogeneous linewidths of low numbers of emitters. This is especially relevant to the understanding of optical quantum states dynamics in nanostructured materials and to their application to quantum technologies.

The PE echo sequence is depicted in Fig.1(a) in the case of well-defined phases $X - Y - X$ for all pulses and an evolution time $2\tau \ll T_2$. For clarity, we also assume $T_2 \ll T_1$, where T_1 is the excited state population lifetime. The first pulse creates superposition states in an inhomogeneously broadened ensemble of emitters and corresponds to a $\pi/2$ rotation along the X axis of the Bloch sphere. After a free evolution time τ , a second pulse rotates the states by an angle π along the Y axis and reverses the phase evolution of the emitters' states. After a second period of free evolution, all states are back in phase at time 2τ and align with the Y axis. The coherent echo emission should take place at this time but instead, a third $\pi/2$ pulse along X is applied which sends the emitters to the excited state (Fig. 1(a)). They afterwards relax by spontaneous emission which is integrated over the excited state population decay.

When the delay τ is increased, more and more emitters are randomly perturbed which results in a lower coherence at the echo time and shorter Bloch vector along Y . After the last $\pi/2$ pulse the excited state population is

also decreasing and ultimately reduces to the center of the Bloch sphere, i.e. equal populations in the excited and ground states. Fig. 1(b) shows a simulation of the distribution of the integrated fluorescence intensity I_{fluor} at $2\tau = 0$ and $2\tau = 3T_2$, adding noise to take into account detector dark counts for example. As expected, I_{fluor} mean value decreases as a function of 2τ and its distribution has a constant width.

The sequence shown in Fig. 1(c) corresponds to the case where the second and third pulses have phases ψ and ϕ that randomly vary from shot to shot with respect to the first pulse phase, arbitrarily chosen as X . In this case, the final state after the last $\pi/2$ pulse is a random vector in the Bloch sphere, and the resulting distribution of I_{fluor} , given by the projection of the vector on the vertical axis, is shown in Fig. 1(d). In opposition to the case of fixed phases, the mean fluorescence intensity is constant whereas the distribution width decreases with increasing evolution time. This suggests that the variance of the fluorescence intensity can be used to retrieve the PE decay and thus the coherence lifetime of the emitters.

Assuming an exponential echo decay of the form $I_{\text{echo}} = I_0 \exp[-2(2\tau/T_2)]$, the integrated fluorescence in-

tensity for sequence (c) reads:

$$I_{\text{fluo}} = \frac{N [1 + \exp(-2\tau/T_2) \cos(\pi - 2\psi + \phi)]}{2}, \quad (1)$$

where N is the number of emitters. For random distributions of the ϕ and ψ angles, and in the absence of additional noise, this leads to the mean and variance of I_{fluo} :

$$m(I_{\text{fluo}}) = N/2 \quad (2)$$

$$\sigma^2(I_{\text{fluo}}) = \frac{N^2 \exp[-2(2\tau/T_2)]}{8}. \quad (3)$$

T_2 can thus be determined by recording $\sigma^2(I_{\text{fluo}})$ even with a laser incoherent over the time range of the PE decay. It is equivalent to monitoring I_{fluo} in the case of fixed phases. Indeed, in sequence (a), $\psi = \pi/2$ and $\phi = 0$ so that $m(I_{\text{fluo}}) = N [1 + \exp(-2\tau/T_2)]/2$ and $\sigma^2(I_{\text{fluo}}) = 0$. Simulated decays of $m(I_{\text{fluo}})$ and $\sigma^2(I_{\text{fluo}})$ in the two cases are presented in Fig. 1(e,f). We note that $\sigma^2(I_{\text{fluo}})$ decays as a function of 2τ as the intensity of the directly detected echo [14].

We next experimentally investigated this method using a 10 ppm doped $\text{Er}^{3+}:\text{Y}_2\text{SiO}_5$ crystal. Part of the setup is shown in the inset of Fig. 2(a). The sample was cut as a polished slab with a thickness of $500 \mu\text{m}$ and cooled to 3.5 K in a closed-cycle cryogenerator, with a permanent magnet producing a field of 200 mT. Excitation was provided by a tunable extended cavity diode laser with no active stabilization. A fluorescence microscopy arrangement was used to excite and collect emission from Er^{3+} ions through a high numerical aperture lens. A single photon InGaAs avalanche photodiode was used for detection and synchronized optical choppers protected the detector from the laser pulses and cut laser stray light during detection. Fluorescence was collected from about 2500 ions and integrated over 40 ms after a delay of 3 ms which was needed to avoid laser leaks due to choppers' jitter. More details can be found in the Supplemental Material (SM).

Fig. 2(a) shows the fluorescence decay obtained by exciting Er^{3+} ions in site 1 of Y_2SiO_5 at 1536.471 nm (vacuum) during $8 \mu\text{s}$. This wavelength corresponds to the ${}^4\text{I}_{15/2}(0) \rightarrow {}^4\text{I}_{13/2}(0)$ transition between the lowest crystal field levels of the excited and ground multiplets [25]. Thanks to pulsed excitation and gated detection, fluorescence could be collected on all ${}^4\text{I}_{13/2}(0) \rightarrow {}^4\text{I}_{15/2}(0-7)$ transitions. An exponential fit of the decay gives $T_1 = 11.0 \pm 0.1$ ms, confirming the origin of the emission [25] and long enough to allow using optical choppers for strongly suppressing laser light.

An excitation spectrum was then recorded by integrating fluorescence decays (Fig. 2(bottom)). It shows four groups of lines that are due to the electronic Zeeman splitting of the ${}^4\text{I}_{13/2}(0)$ ($g \approx 10.5$) and ${}^4\text{I}_{15/2}(0)$ ($g \approx 7.0$) levels [26]. Additional lines were observed for

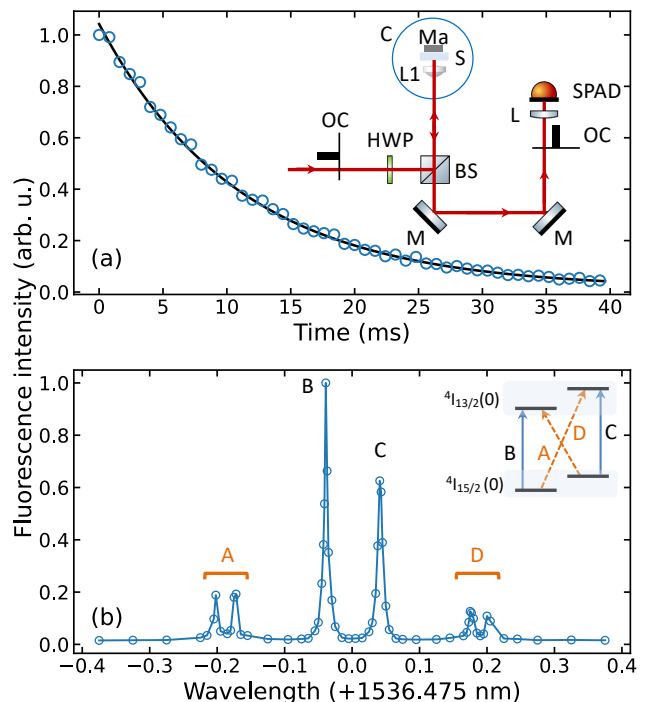


FIG. 2. Fluorescence properties of Er^{3+} ions in Y_2SiO_5 (site 1) at 3.5 K. (a) Fluorescence decay of the ${}^4\text{I}_{13/2} \rightarrow {}^4\text{I}_{15/2}$ transition excited at 1536.471 nm (vac.) and exponential fit (black line) giving $T_1 = 11.0 \pm 0.1$ ms. (inset) Schematic of fluorescence microscopy setup. OC: optical chopper, HWP: half-wave plate, BS: beam splitter, L1, L: lenses, S: sample, C: cryostat, Ma: Magnet, SPAD: single-photon avalanche photodiode. (b) Excitation spectrum of the ${}^4\text{I}_{15/2}(0) \rightarrow {}^4\text{I}_{13/2}(0)$ transition with light polarized along the b axis and magnetic field $\mathbf{B} \parallel D2$. Wavelength in vacuum. The A-D lines are due to Zeeman splittings in the ground and excited states (inset and main text).

the A and D groups and assigned to magnetically non-equivalent sites related by a C_2 rotation of the crystal unit cell. From the positions to the lines and known g tensors, the field amplitude was determined at 200 mT and in a direction slightly away from the crystal $D2$ axis. Echo experiments were performed on the B line which has an inhomogeneous linewidth of about 0.7 GHz.

Next, we first used a delay $\tau = 0.8 \mu\text{s}$ to record fluorescence-detected photon echoes as depicted in Fig. 1(a). Indeed, for such short delays, the laser coherence is sufficient to preserve relative phases between the three pulses. A plot of $m(I_{\text{fluo}})$ as a function of the last $\pi/2$ pulse phase ϕ is shown in Fig. 3(a). Each data point was averaged over 1000 shots. A cosine variation was observed in agreement with Eq. 1, which confirmed that an echo signal was indeed detected by fluorescence. Further proof was given by experiments carried out on a larger sample for which echoes could be directly detected (see SM). Moreover, by repeating the fixed phase experiment

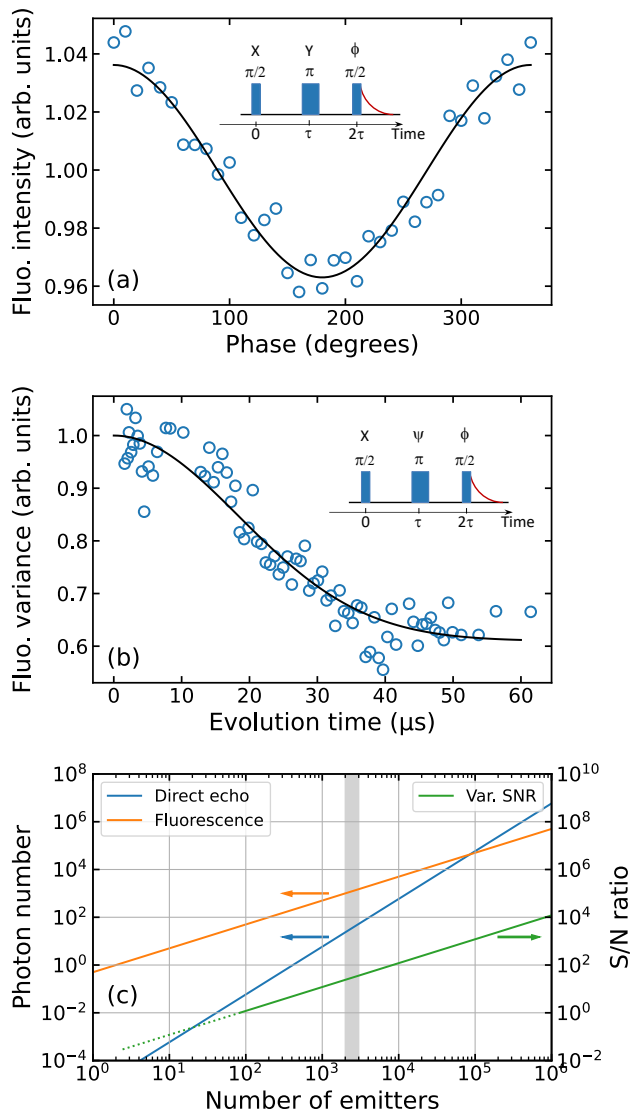


FIG. 3. Fluorescence-detected photon echoes. (a) Variation of $m(I_{\text{flu}})$ as a function of phase ϕ and fit with a cosine function (see text). Inset: pulse sequence, $2\tau = 1.6 \mu\text{s}$. (b) $\sigma^2(I_{\text{flu}})$ as a function of the evolution time 2τ with random phases ψ and ϕ . Inset: pulse sequence. A fit with a stretched exponential ($\beta = 2$) gives $T_2 = 37 \pm 2 \mu\text{s}$ (black line). (c) Theoretical integrated intensities for fluorescence-detected (orange) and direct (blue) echoes for unit collection efficiencies and this work's experimental parameters. Green line: signal to noise ratio for the fluorescence intensity variance (see text). Gray vertical area: estimated number of ions in (a) and (b). Arrows denote relevant vertical scales.

for increasing delays τ , we found a laser coherence lifetime $T_{2,\text{laser}} = 15 \pm 1 \mu\text{s}$ or $\Gamma_{\text{laser}} = 21 \pm 2 \text{kHz}$ (see SM). As seen in Fig. 3(a), the peak-to-peak variation of $m(I_{\text{flu}})$ vs. ϕ was about 8% of the mean value. This is mainly attributed to an inhomogeneous Rabi frequency across the ions because of the small frequency range addressed by the laser (1 MHz) compared to the transition

inhomogeneous broadening (0.7 GHz).

Echo decays were finally recorded using $\sigma^2(I_{\text{flu}})$, following the scheme presented in Fig. 1(c). To avoid different time regimes of laser stability, we randomized the phases of the pulses through the digital waveforms used to create them. The variance was calculated from 2000 shots for each delay τ at a repetition rate of 10 Hz. Fluorescence intensity varied from shot to shot by a few % for a given delay, indicating good short-term stability of the experiment and the lack of spectral hole burning. For each delay, about 200 outlier values (larger than 5 standard deviations), attributed to synchronization issues with the choppers and counting system, were observed and discarded.

A clear decay of $\sigma^2(I_{\text{flu}})$ as a function of 2τ was observed corresponding to a coherence lifetime of $37 \pm 2 \mu\text{s}$ according to a stretched exponential fit (Fig. 3(b)). This is in qualitative agreement with the expected value under our conditions of temperature and magnetic field. The main decoherence process is attributed to spectral diffusion due to the Er^{3+} spin bath [16, 27]. The optical setup did not allow to directly record the photon echo because of the several ms delay between the last $\pi/2$ pulse and the opening of the detection window. We could however confirm that $\sigma^2(I_{\text{flu}})$ decay was identical to the one obtained by direct detection of the echo on the larger sample mentioned above (see SM).

The results presented above were obtained on a small number of ions. The latter will be typically located within a sub-wavelength volume (a single particle or thin film) or coupled to an optical resonator or waveguide so that the collection efficiencies of the direct and fluorescence-detected echoes are equal. In the following, we consider them equal to 1 for simplicity. The directly detected integrated echo signal for N ions and $2\tau \ll T_2$ is then given by [24]:

$$I_{\text{echo}} = \frac{N^2 A_{sp} \tau_{\text{echo}}}{4} \quad (4)$$

where A_{sp} is the spontaneous emission rate on the echo transition and τ_{echo} is the echo pulse length. This formula is valid in the case of low absorption where echo absorption and amplification can be neglected and for $A_{sp} \tau_{\text{echo}} \ll 1$. Fluorescence detection gives $I_{\text{flu}} = N/2$ and is ≈ 40 times larger than I_{echo} in our experiments ($N = 2500$, $A_{sp} = 27 \text{s}^{-1}$ [25], and $\tau_{\text{echo}} = 800 \text{ns}$) as shown in Fig. 3(c). The ratio $I_{\text{flu}}/I_{\text{echo}}$ is proportional to N , evidencing the interest of fluorescence detection for small ensembles of emitters.

The lower bound on N can be evaluated by estimating the noise affecting $\sigma^2(I_{\text{flu}})$. For low N it is dominated by the fluorescence intensity shot-noise, which has a variance of $\sigma_{\text{noise}}^2(I_{\text{flu}}) = N/2$. If n experimental values are used to compute $\sigma^2(I_{\text{flu}})$, the standard deviation on $\sigma_{\text{noise}}^2(I_{\text{flu}})$ is $N/\sqrt{2n}$ for $n, N/2 \gg 1$. The signal-to-noise ratio at $2\tau \ll T_2$ is then propor-

tional to N : $R = k^2 N \sqrt{n/32}$, where k , defined by $\sigma^2(I_{\text{fluo}}) = k^2 N^2/8$, takes into account the inhomogeneous Rabi frequency effect.

In the experiments presented above, $k = 0.04$ (Fig. 3(c)) and SM) and $n = 1800$, giving a lower bound $N = 84$ for $R = 1$. This evaluation assumes that other sources of noise related to excitation and detection are negligible compared to the shot-noise contribution. To further decrease N or increase R , k could be improved by creating an ensemble of emitters with a linewidth comparable to the excitation bandwidth inside a larger non-absorbing region. This can be done using spectral hole burning techniques and results in much better Rabi frequency homogeneity [28]. It is important to note that at least two emitters are required for the method to work since otherwise there is no distinction between decoherence and random laser pulse phases. The condition $T_{2,\text{laser}} \gg T_2$ is therefore needed for fluorescence-detected photon echoes on single ions [11].

In conclusion, we have shown that photon echoes can be created and detected using an excitation source and detection that are both incoherent on the time scale of the experiment. This is achieved by converting the echo into populations with an additional laser pulse and measuring the subsequent integrated fluorescence intensity variance instead of its mean value. We demonstrate the validity of the concept using an $\text{Er}^{3+}:\text{Y}_2\text{SiO}_5$ crystal in which we record an echo decay leading to a coherence lifetime $T_2 = 37 \pm 2 \mu\text{s}$ ($\Gamma_h = 8.6 \pm 0.4 \text{ kHz}$) whereas $T_{2,\text{laser}} = 15 \pm 1 \mu\text{s}$ ($\Gamma_{\text{laser}} = 21 \pm 2 \text{ kHz}$). Furthermore, these data were acquired using about 2500 ions, which shows the potential of this method to work with small ensembles of emitters, with a shot-noise limited lower limit estimated in our system below 100 ions. This in turn should enable one to fully benefit from the robustness and multi-timescale capability of the photon echo technique to efficiently assess the coherence dynamics of nanostructured materials that find applications in quantum nanophotonics.

This project has received funding from the European Research Council (ERC) under the European Union's Horizon 2020 research and innovation programme (RareDiamond, grant agreement No 101019234) and the French Agence Nationale de la Recherche under grants ANR-20-CE09-0022 (UltraNanoSpec) and ANR-23-CE47-0011 (MolEQuBe), and the Plan France 2030 project ANR-22-PETQ-0010 (QMemo).

* philippe.goldner@chimieparistech.psl.eu

- [1] C. W. Thiel, T. Böttger, and R. L. Cone, Rare-earth-doped materials for applications in quantum information storage and signal processing, *Journal of Luminescence* **131**, 353 (2011).
 [2] M. Le Dantec, M. Rančić, S. Lin, E. Billaud, V. Ran-

- jan, D. Flanigan, S. Bertaina, T. Chanelière, P. Goldner, A. Erb, R. B. Liu, D. Estève, D. Vion, E. Flurin, and P. Bertet, Twenty-three-millisecond electron spin coherence of erbium ions in a natural-abundance crystal, *Science Advances* **7**, eabj9786 (2021).
 [3] M. Rancic, M. P. Hedges, R. L. Ahlefeldt, and M. J. Sellars, Coherence time of over a second in a telecom-compatible quantum memory storage material, *Nature Physics* **14**, 50 (2018).
 [4] M. Zhong, M. P. Hedges, R. L. Ahlefeldt, J. G. Bartholomew, S. E. Beavan, S. M. Wittig, J. J. Longdell, and M. J. Sellars, Optically addressable nuclear spins in a solid with a six-hour coherence time, *Nature* **517**, 177 (2015).
 [5] S. Gupta, Y. Huang, S. Liu, Y. Pei, N. Tamm, R. J. Warburton, and T. Zhong, Dual epitaxial telecom spin-photon interfaces with correlated long-lived coherence (2023), arXiv:2310.07120 [quant-ph].
 [6] M. Businger, L. Nicolas, T. S. Mejia, A. Ferrier, P. Goldner, and M. Afzelius, Non-classical correlations over 1250 modes between telecom photons and 979-nm photons stored in $171\text{Yb}^{3+}:\text{Y}_2\text{SiO}_5$, *Nature Communications* **13**, 6438 (2022).
 [7] D. Lago-Rivera, S. Grandi, J. V. Rakonjac, A. Seri, and H. de Riedmatten, Telecom-heralded entanglement between multimode solid-state quantum memories, *Nature* **594**, 37 (2021).
 [8] X. Liu, X.-M. Hu, T.-X. Zhu, C. Zhang, Y.-X. Xiao, J.-L. Miao, Z.-W. Ou, P.-Y. Li, B.-H. Liu, Z.-Q. Zhou, C.-F. Li, and G.-C. Guo, Nonlocal photonic quantum gates over 7.0 km, *Nature Communications* **15**, 8529 (2024).
 [9] J. G. Bartholomew, J. Rochman, T. Xie, J. M. Kindem, A. Ruskuc, I. Craiciu, M. Lei, and A. Faraon, On-chip coherent microwave-to-optical transduction mediated by ytterbium in YVO_4 , *Nature Communications* **11**, 3266 (2020).
 [10] S. Ourari, L. Dusanowski, S. P. Horvath, M. T. Uysal, C. M. Phenicie, P. Stevenson, M. Raha, S. Chen, R. J. Cava, N. P. de Leon, and J. D. Thompson, Indistinguishable telecom band photons from a single Er ion in the solid state, *Nature* **620**, 977 (2023).
 [11] J. M. Kindem, A. Ruskuc, J. G. Bartholomew, J. Rochman, Y. Q. Huan, and A. Faraon, Control and single-shot readout of an ion embedded in a nanophotonic cavity, *Nature* **580**, 201 (2020).
 [12] C. Deshmukh, E. Beattie, B. Casabone, S. Grandi, D. Serrano, A. Ferrier, P. Goldner, D. Hunger, and H. de Riedmatten, Detection of single ions in a nanoparticle coupled to a fiber cavity, *Optica* **10**, 1339 (2023).
 [13] A. Gritsch, L. Weiss, J. Früh, S. Rinner, and A. Reiserer, Narrow Optical Transitions in Erbium-Implanted Silicon Waveguides, *Physical Review X* **12**, 041009 (2022).
 [14] P. Goldner, A. Ferrier, and O. Guillot-Noël, Rare Earth-Doped Crystals for Quantum Information Processing, in *Handbook on the Physics and Chemistry of Rare Earths*, Vol. 46, edited by J.-C. G. Bünzli and V. K. Pecharsky (Elsevier, Amsterdam, 2015) pp. 1–78.
 [15] N. A. Kurnit, I. D. Abella, and S. R. Hartmann, Observation of a Photon Echo, *Physical Review Letters* **13**, 567 (1964).
 [16] T. Böttger, C. W. Thiel, Y. Sun, and R. L. Cone, Optical decoherence and spectral diffusion at 1.5 $M\mu\text{m}$ in $\text{Er}^{3+}:\text{Y}_2\text{SiO}_5$ versus magnetic field, temperature, and Er^{3+} concentration, *Physical Review B* **73**, 075101

- (2006).
- [17] R. M. Macfarlane, High-resolution laser spectroscopy of rare-earth doped insulators: A personal perspective, *Journal of Luminescence* **100**, 1 (2002).
- [18] L. Weiss, A. Gritsch, B. Merkel, and A. Reiserer, Erbium dopants in nanophotonic silicon waveguides, *Optica* **8**, 40 (2021).
- [19] L. Allen and J. H. Eberly, *Optical Resonance and Two-Level Atoms* (Dover, 1987).
- [20] T. Zhong and P. Goldner, Emerging rare-earth doped material platforms for quantum nanophotonics, *Nanophotonics* **8**, 2003 (2019).
- [21] A. Fossati, S. Liu, J. Karlsson, A. Ikesue, A. Tallaire, A. Ferrier, D. Serrano, and P. Goldner, A Frequency-Multiplexed Coherent Electro-optic Memory in Rare Earth Doped Nanoparticles, *Nano Letters* **20**, 7087 (2020).
- [22] A. Ulanowski, B. Merkel, and A. Reiserer, Spectral multiplexing of telecom emitters with stable transition frequency, *Science Advances* **8**, eabo4538 (2022).
- [23] B. Car, L. Veissier, A. Louchet-Chauvet, J.-L. Le Gouët, and T. Chanelière, Selective Optical Addressing of Nuclear Spins through Superhyperfine Interaction in Rare-Earth Doped Solids, *Physical Review Letters* **120**, 197401 (2018).
- [24] E. Billaud, L. Balembois, M. Le Dantec, M. Rančić, E. Albertinale, S. Bertaina, T. Chanelière, P. Goldner, D. Estève, D. Vion, P. Bertet, and E. Flurin, Microwave Fluorescence Detection of Spin Echoes, *Physical Review Letters* **131**, 100804 (2023).
- [25] T. Böttger, Y. Sun, C. W. Thiel, and R. L. Cone, Spectroscopy and dynamics of Er³⁺:Y₂SiO₅ at 1.5 μm, *Physical Review B* **74**, 075107 (2006).
- [26] Y. Sun, T. Böttger, C. W. Thiel, and R. L. Cone, Magnetic g tensors for the 4I_{15/2} and 4I_{13/2} states of Er³⁺:Y₂SiO₅, *Physical Review B* **77**, 085124 (2008).
- [27] B. Car, J.-L. Le Gouët, and T. Chanelière, Superhyperfine induced photon-echo collapse of erbium in Y₂SiO₅, *Physical Review B* **102**, 115119 (2020).
- [28] O. Guillot-Noël, P. Goldner, F. Beaudoux, Y. Le Du, J. Lejay, A. Amari, A. Walther, L. Rippe, and S. Kröll, Hyperfine structure and hyperfine coherent properties of praseodymium in single-crystalline La₂(WO₄)₃ by hole-burning and photon-echo techniques, *Physical Review B* **79**, 155119 (2009).